Advancing Control Methods for Biohybrid Microrobots: A Focus on Vertical Rolling Locomotion

Joep K. van der Mijle Meijer

Abstract— **The field of Biomedical Engineering has given high praise to the research topic of microrobots and biohybrid types in particular. Their promising application in targeted drug delivery for cancer treatments fuels the search for the optimal design. Currently, magnetic biohybrid microrobots receive a lot of attention. This paper will investigate magnetically actuated nanoparticle-coated sperm cell clusters or IRONSperm. The control of IRONSperm clusters has been researched in multiple studies, showing an excellent response to a rotating permanent magnet. Vertical locomotion has not yet been explored and would frame the potential of IRONSperm for clinical use. This paper thus researched the differences between ceiling- and side-rolling of vertical rolling locomotion for IRONSperm. A negligible effect was found of the inclination angle upon the speed of the cluster. Increasing actuation distance resulted in slightly lower velocities of the cluster until it was not able to follow. Ceiling rolling was found to perform quicker in a positively inclined situation while side rolling proved to be the most appropriate method for horizontal and descending trajectories. Using these two methods, the IRONSperm cluster was successfully able to navigate through all branches of a trifurcation phantom. This result was also validated with successful trajectories through an anatomically accurate phantom of the female reproductive tract. These experiments proved the potential of RPM-actuated control of IRONSperm clusters in closed vessels. Further research should focus on methods to overcome the short actuation distance problem and closed-loop control schemes.**

I. INTRODUCTION

Annually, more than 142.000 cases and approximately 225.000 cases were reported for endometrial and ovarian cancer respectively, making it the 6th and 8th most common cancers in women. The treatments currently rely on a combination of surgical cytoreduction and adjuvant chemotherapy. [1], [2] This treatment only accounts for a 5 year survival rate below 50% for ovarian cancer and approximately 75% for endometrial cancer [3], [4]. Soft biohybrid microrobots have sparked a new interest within the field of biomedical engineering because of their promising application in targeted drug delivery, local hypothermia generation and cell microsurgery. [5]. Their compact design in combination with suitable biocompatibility is observed as highly desirable for these intended purposes. Biohybrid microrobots possess the ability to reach cavities and small spaces which current targeted robots have not been able to achieve. Thus far, various articles have proposed several methods of actuation and sensing techniques [6]–[10]. Magnetic control has received high praise over chemical, electrical and optical methods due to the absence of chemical interaction and excellent external control with high actuation distances [11]. Magnetic actuation offers a wide range of locomotion principles, featuring gradient pulling, helical propulsion, flagellar propulsion and surface rolling [12]. Most of these can be achieved by electromagnets and permanent magnets, both providing their specific set of advantages and limitations. The use of coils for magnetic actuation provides more accurate control in 5 degrees of freedom (DOF). However, precise actuation is proportional to the number of coils and the production of heat, therefore often not favored in surgical settings. Rotating permanent magnets (RPM) have been shown to safely control microrobots through magnetic torque and friction with a rolling surface. Despite its success with several microrobots, the control scheme relies on feedback for accurate control which is often difficult to provide [13]–[16]. Open loop testing is therefore preferred to express the clinical relevance of the system. Challenges in full control remain present for microrobots in all forms. One of these is the ability to reach automated control in 5 DOF, three translational and two rotational dimensions. The potential for automated control lies in the realisation of full dimensional control, including vertical locomotion. Most locomotion techniques explained above are constrained by their necessity to overcome gravitational and viscous drag forces to preserve vertical position. This, in turn, compromises the efficiency of the intended motion, since the compensation for descent reduces speed in the desired direction.

Rolling locomotion does not abide by this force compensation since it remains in contact with a rolling surface. This eliminates the necessity for the microrobot to remain in the free space of the cavity to avoid collisions with any surfaces it may encounter. Recently, Middelhoek et al have developed magnetic non-motile sperm clusters (IRONSperm), which demonstrated the potential of surface-rolling microrobots for targeted drug delivery [17]. Nonetheless, this potential has yet to be assessed. Braks researched the limitations of the rolling behaviour of IRONSperm, concluding that vertical movement is strongly correlated with the actuation distance, the distance between cluster and RPM, and magnetic field strength [18]. Since magnetic field strength exerted on the cluster can be increased by decreasing actuation distance, the main focus relies on the effect of the latter. The ease at which magnetic field strength can be amplified by either changing magnet size or decreasing actuation distance poses the question what the trade-off would be. Braks suggested that the workspace of the robot would be a limiting factor in comparison with the space where the cluster is supposed

to move in [18].

This study aims to research the most appropriate methods for vertical locomotion of IRONSperm clusters in terms of performance and robot manoeuvrability. The work shall propose what methods will be investigated and which pose the best compromise between cluster speed and robot movement in a two-dimensional vertical plane.

II. Theoretical Background

A. Cluster formation

Individual bovine sperm cells are dipped in a suspension of iron magnetic nanoparticles (MNP's) with a diameter of approximately 15 nm. The negatively charged sperm cells and positively charged MNP's self-assemble through electrostatic interactions. According to Magdanz et al (2020), the self-assembly process allows for heterogeneity in the distribution of MNP's among the membrane of the sperm cells [19]. This results in the formation of differentiated IRONSperm, thus responding differently to an applied magnetic field. However, when IRONSperm entangles, they form clusters in the process, removing this heterogeneity problem. The clusters are further aggregated through a rotating magnetic field, fusing smaller clusters into one big cluster [20].

B. Actuation Methodology

The IRONSperm clusters are actuated by an external rotating permanent magnet (RPM). The magnetic dipole moment of the clusters aligns with the applied magnetic field induced by this RPM. The rotation of the magnet thus causes the cluster to mimic its motion in an attempt to remain aligned with the magnetic field. As a result, this causes the IRONSperm clusters to engage in rolling locomotion along a surface. The magnet is coupled to a Maxon 18 V brushless DC motor with a gear ratio of 3.7:1. The motor is then mounted upon a KUKA 6-DOF manipulator (KUKA KR-10 1100-2, KUKA, Augsburg, Germany), allowing for movement of the magnet in any arbitrary trajectory [20].

C. Magnetic torque and forces

As explained in the previous section, the rolling locomotion is achieved by the alignment to a rotating magnetic field. The resulting form of locomotion is rolling, caused by magnetic torque induced as a result of the force pushing the cluster to rotate around its axis on a rolling surface. Since the target environment for the application of IRONSperm will occur in low Reynolds number conditions, the following force balance is used to describe the cluster's behaviour [21].

$$\begin{pmatrix} \mathbf{F}_\mathrm{m} + \mathbf{F}_\mathrm{d} + \mathbf{F}_\mathrm{f} \\ \boldsymbol{\tau}_\mathrm{m} + \boldsymbol{\tau}_\mathrm{d} + \boldsymbol{\tau}_\mathrm{f} \end{pmatrix} = 0, \tag{1}$$

Where $\mathbf{F}_\mathrm{m}$ is the magnetic force applied between two clusters. $\mathbf{F}_\mathrm{d}$ is the viscous drag force given by the formula $\mathbf{F}_\mathrm{d} = \mathrm{f_t}\mathbf{v}$ where $\mathrm{f_t}$ is the translational drag coefficient and $\mathbf{v}$ the velocity of the cluster. $\mathbf{F}_\mathrm{f}$ is the frictional force exerted on the cluster. Furthermore, $\boldsymbol{\tau}_\mathrm{m}$, $\boldsymbol{\tau}_\mathrm{d}$ and $\boldsymbol{\tau}_\mathrm{f}$ are the magnetic, drag and frictional torques necessary to complete the motion behaviour. The magnetic torque is given by $\boldsymbol{\tau}_m = \mathbf{m} \times \mathbf{B}$, where $\mathbf{m}$ is the magnetic moment and $\mathbf{B}$ is the magnetic field. Finally, the viscous drag torque is calculated using $\boldsymbol{\tau}_\mathrm{d} = \mathrm{f_r}\omega_\mathrm{c}$. In this formula, $\mathrm{f_r}$ is the rotational drag coefficient and ω_c is the angular velocity of the cluster. [17] Depending on the actuation distance, a cluster is either able to travel along the surface closest to the RPM or the opposite surface (Appendix A) [20]. The pulling force allows for a larger frictional force and has been shown to increase tracking speed rather than bottom floor locomotion [18].

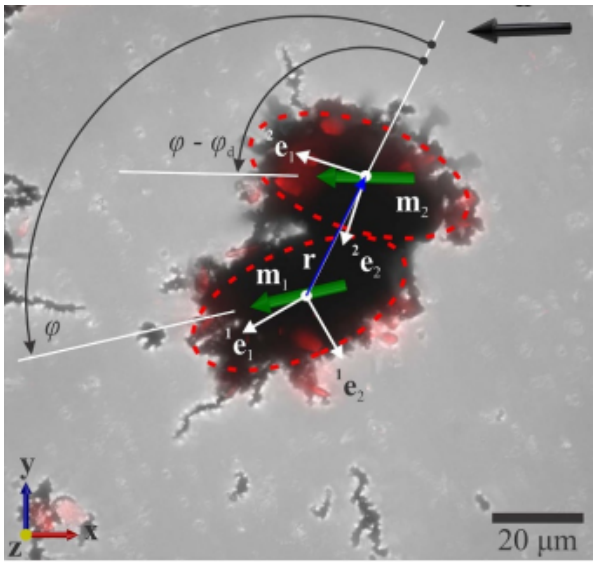

Fig. 1: Two clusters at distance r aggregate under the influence of a rotating magnetic field, fusing into one big cluster. [17]

D. Disassembly of clusters

During the rotation of the cluster, several forces act on the body. All of these forces can be described using Equation 1. In the event where the external forces overpower the forces between individual IRONSperm in the cluster, it will start to decompose. Weber noted that this disassembly of clusters is a recurring problem for the reproduction of results with IRONSperm, obstructing the possibility of quantifying the behaviour of IRONSperm under different conditions [22]. To understand the breaking and agglomerating of IRONSperm clusters, some forces should be considered more carefully.

The force that exists between two separate clusters is given by:

$$\mathbf{F_m} = \frac{3\mu_0}{4\pi|\mathbf{r}|^4}(\mathbf{m_2}(\mathbf{m_1}\cdot\hat{\mathbf{r}}) + \mathbf{m_1}(\mathbf{m_2}\cdot\hat{\mathbf{r}}) + \hat{\mathbf{r}}(\mathbf{m_1}\cdot\mathbf{m_2}) - 5\hat{\mathbf{r}}(\mathbf{m_1}\cdot\mathbf{r})(\mathbf{m_2}\cdot\hat{\mathbf{r}})), \tag{2}$$

where $\mathbf{m}$ is the magnetic moment of a cluster, $\hat{\mathbf{r}}$ is the unit vector between the clusters and $|\mathbf{r}|$ is the distance

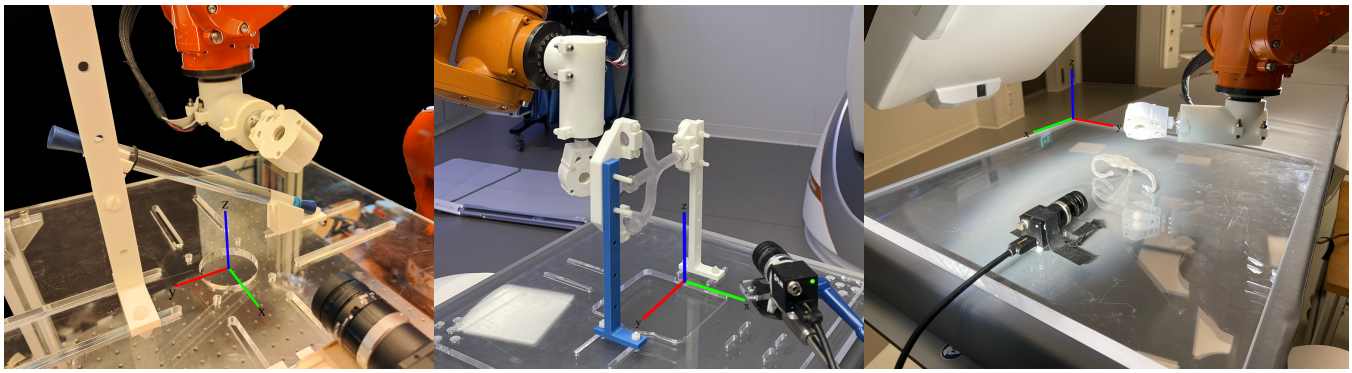

(a) (b) (c)

Fig. 2: Perspex tube in inclined situation (a), Trifurcation phantom in vertical position (b) and reproductive tract phantom (c) under visual feedback from a FLIR Blackfly camera (Teledyne FLIR LLC, Willsonville, Oregon), and a C-arm for x-ray and CB-CT imaging.

between them. This force is only applicable when clusters are relatively close together as seen in Figure 1.

Under very high actuation frequencies, clusters start to break down as a result of the friction exerted by the solid boundary and the centrifugal force acting on the cluster [18]. Separate clusters roll synchronously with the RPM under the influence of the force given in Equation 2. These clusters may adopt different speeds according to size and shape, thus impeding the agglomeration of them.

E. Localisation of clusters

Prior research has shown that IRONSperm clusters are difficult to localise using the existing imaging techniques. Studies by Middelhoek et al and Bloxs have shown that ultrasound is the preferred imaging modality to detect and evaluate the position of IRONSperm clusters [17] [23]. This inexpensive technique provided successful trials for localisation but shows poor Contrast to Noise Ratio (CNR) and image quality. Furthermore, the localisation technique was investigated under a maximum actuation frequency of 1 Hz at a speed of 1 mm s^{-1}. The values for these parameters of the current clusters lie much higher as shown by Braks and Weber [18] [22]. Therefore the image quality is expected to only decrease further, subsequently impeding the ability to localise the cluster for *in vivo* applications.

Other imaging techniques have therefore been proposed such as X-ray and Magnetic Particle Imaging. Magnetic Particle Imaging is a new tomographic technique based on the tracing of superparamagnetic particles in a gradient magnetic field [24]. This technique would allow for simultaneous actuation and localisation but might interfere between RPM and the imaging device. X-ray uses radiation and therefore is not preferred for this research, since dosage would be excessive for real-time imaging.

Cone Beam Computed Tomography or CB-CT scanning is therefore used to quantify the starting and end position in an open-loop response of the clusters. The proposed method in this investigation is research-based only and thus does not provide clinical relevance.

F. Reproductive tract viability

Due to the combination of biological and artificial components in IRONSperm, the construct shows excellent cytocompatibility [25]. Thus the clusters will not harm the reproductive tract. The 0.9% medical saline solution used for the trials shows comparable characteristics to the fluid in the uterus and fallopian tubes [26] [27]. The hair structures in the fallopian tubes called cilia provide a peristaltic motion to propel a zygote towards the uterus. This is initiated upon sensing an object. The cilia also provide aid in the disintegration of sperm cells when entangled [28].

III. Methodology

A. Assembly of IRONSperm

Nanoparticle-coated bull sperm cells were fabricated by electrostatic-based self-assembly [6]. A 500 μL suspension of a sperm cell concentration of 2.5 × 10^7 cells/mL was added to a microcentrifugation tube each. 150 µL of iron oxide (Fe_3O_4) nanoparticles solution 10 mg/mL is added to the tube, resulting in a nanoparticle concentration of 3 mg/mL combined with the sperm.

B. Slope angle and actuation distance

To investigate and quantise the vertical rolling capabilities of IRONSperm, its response was tested under sloped surfaces of different angles. One IRONSperm cluster was considered for all trials and was placed in a transparent perspex tube filled with 0.9% saline solution. 5 angles were tested during this experiment from 15 to 75 degrees with steps of 15 degrees each. For each angle, 5 trials were conducted, each with a different actuation distance. These ranged from 37.5 to 47.5 mm distance between the RPM centre and the rolling surface. The magnet used for all trials was a circular actuator magnet (NdFeB Grade-N45) with radius of 17.5 mm and height of 20.0 mm. The RPM travelled in a linear trajectory above the tube over a distance of 180 mm under the respective angles parallel to the tube. The experimental set-up is displayed in Figure 2a

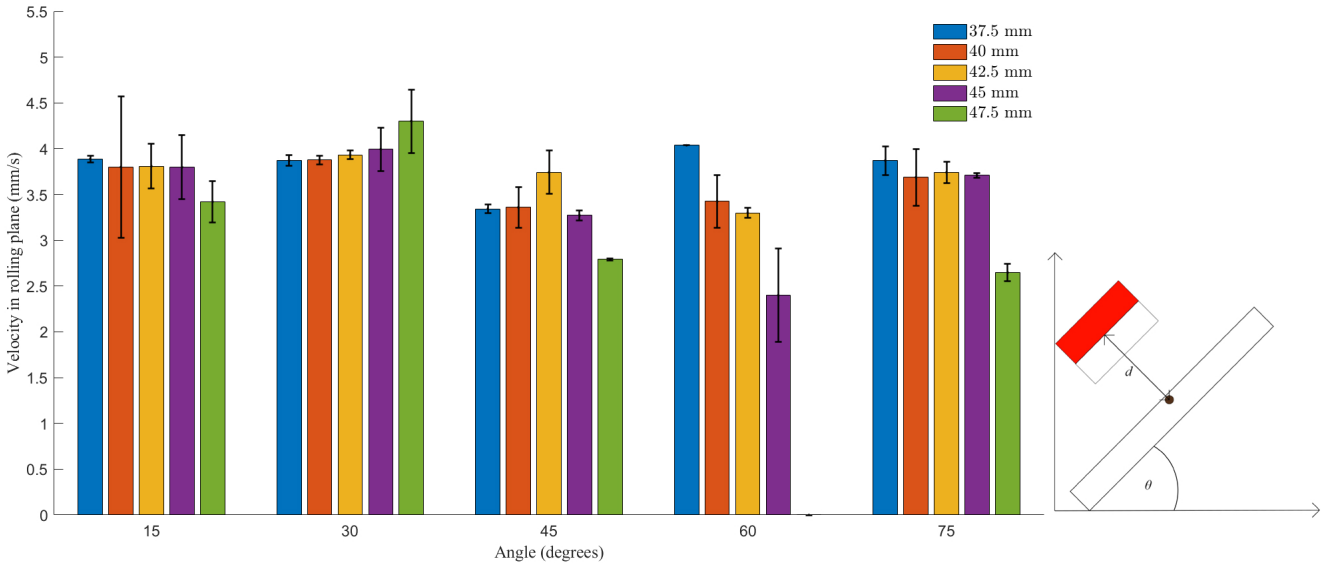

Fig. 3: The effect of the actuation distance (d), denoted by the different colored bars, and the angles (θ), denoted by separate bar groups, on the rolling velocity is depicted.

Trials were repeated threefold. The linear speed of the KUKA remained at 4 mm s^{-1} at which the cluster was able to follow for most angles and distances. During all trials, the rotation frequency of the RPM was kept at 1.5 Hz and the direction was switched upon change of KUKA trajectory. All trials were filmed using a FLIR Blackfly camera at a framerate of 30 frames per second.

C. Side vs ceiling rolling

The difference between side rolling and ceiling rolling over sloped trajectories, both under pulling force influence was investigated using the same set-up seen in the previous section (see Figure 2a). A different cluster was used for this trial of the same concentration, namely 3 mg/mL. The RPM moved laterally and parallel to the tube, with the RPM rotating in the same plane as the cluster over a linear trajectory of 110 mm at a speed of 7 mm s^{-1} to remove the drag effect. Removing this effect isolates the rolling behaviour so rolling velocity can be accurately computed. Three angles were used, starting with a perfect horizontal set-up and increasing the angle to 30 and 60 degrees. Each angle was tested with a 47.5 mm actuation distance.

D. Trifurcation and reproductive tract

Two phantoms are considered to validate the control methods investigated in the prior experiments. The first one is a resin 3D-printed trifurcation phantom. The trifurcation was placed in a YZ-plane as seen in Figure 2b. The RPM realised both ceiling and side rolling for the top branch and side rolling for the middle and lower branches. At least three successful trials were captured for each branch to ensure proof of principle. The desired paths were recorded using a FLIR Blackfly camera at 30 frames per second with a Fujinon 1:1.2/6 mm lens and were also validated with an X-ray set-up.

The second phantom represents an accurate real-size duplicate of the reproductive tract. The reproductive tract was placed in an anatomically accurate position (Figure 2c) to mimic a patient's orientation during an operation. The RPM moved along a trajectory drawn in the RoboDK software above the phantom to manoeuvre the cluster to the fallopian tube. 5 successful trials were recorded for each fallopian tube with both a FLIR Blackfly camera and continuous x-ray. The final position of the cluster was also evaluated in a CB-CT scan of the complete phantom for all successful trials. The set-up as seen in Figure 2c was used for all trials. The trajectories used are displayed in Appendix B

IV. EXPERIMENTAL RESULTS

A. Inclination and actuation distance

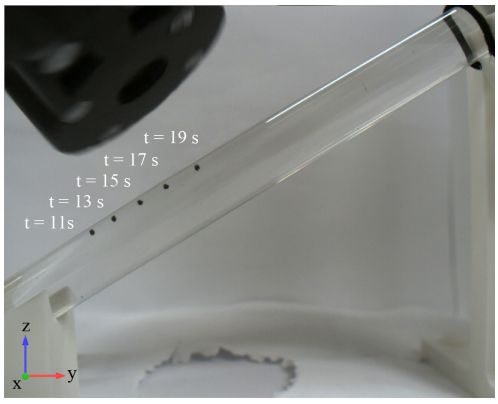

Fig. 4: Rolling locomotion of an IRONSperm cluster under an inclination of 30 degrees at an actuation distance of 37,5 mm

Velocity was analysed using Tracker Video Analysis and Modeling Tool (Version 6.1.5, [29] Brown et al, 2023) and MATLAB (Version 23.2.0 (2023b) [30] The MathWorks Inc., 2023) of which the results are shown in Figure 3 (see Appendix C). The cluster rolls along the slope as shown in Figure 4 The data showed a slight linear regressing pattern of velocity with increasing angle. 37.5 mm actuation remained approximately constant for all angles. In the range of 37.5 - 42.5 mm, measurements showed a minimal decrease in speed for all angles, thus giving the optimal working range for vertical locomotion. Actuation distance showed a clear regressing trend per angle, especially under steeper sloped conditions. During the trials with slope angles of 60 and 75 degrees, the cluster lost magnetic coupling with the RPM at actuation distances in the range of 45 mm- 47.5 mm. This impaired the protocol to complete 3 successful runs for each direction. After about 7 seconds, the RPM would not exert enough pulling force on the cluster to overcome gravity, causing the cluster to drop under its weight. Interestingly, it became clear that magnetic torque was still acting on the cluster since it continued to roll on the opposite surface in the opposite direction.

B. Vertical Locomotion: Two methods

This experiment showed clear differences in the rolling velocity of the cluster on an inclined surface while rolling on the side or ceiling. The average velocities of both methods are displayed in Figure 5. The velocity for side rolling is higher for the angles of 0 and 30 degrees. For higher angles, however, ceiling rolling dominates. Ceiling rolling shows a positive correlation between rolling velocity and inclination, while side rolling shows a declining trend. A test was performed without rotation of the permanent magnet to evaluate the ability of the cluster to track in a dragging motion under the influence of the pulling force. The horizontal set-up resulted in perfect tracking for contact with the ceiling. However, the cluster was not able to follow while in contact with the side of the tube.

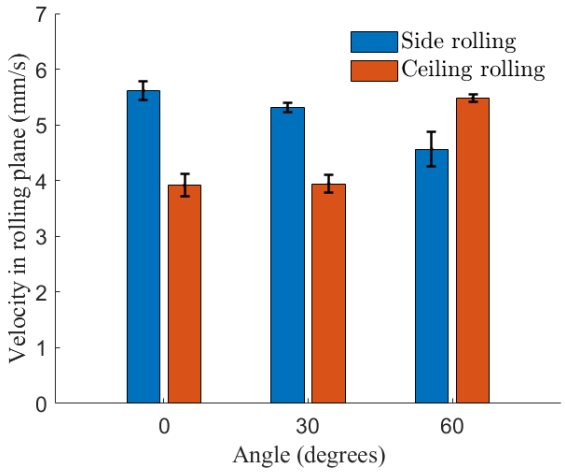

Fig. 5: The velocities of side rolling (blue) and ceiling rolling (red) under different inclination angles are shown.

C. Trifurcation control

The control methods investigated in the previous sections were tested in a trifurcation phantom shown in Section III-D. The lower and middle branches were tested using the side-rolling approach and the top branch was tested using both approaches explained in the previous section IV-B. Each branch and method was run for 3 successful trials of which the trajectories are shown in Figure 7A, C and E. The response to the RPM at a linear speed of 80 mm-s with a joint speed of 60 mm-s proved to be the best combination for the selected paths.

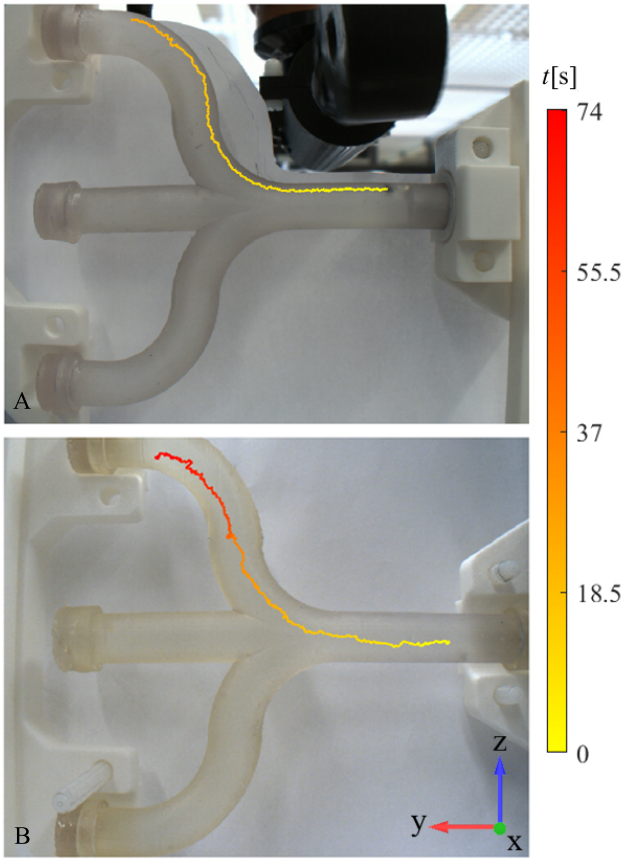

Fig. 6: Top branch cluster paths are shown for ceiling rolling (A) and side-rolling (B) approaches

In Figure 6 the behaviour of ceiling rolling and side-rolling is shown for the top branch. It is clear that ceiling rolling is faster than side-rolling for this trajectory. Side-rolling accounted for a full trajectory time of 74 seconds, starting upon movement in the starting branch and ending upon stationary positional rolling. This trajectory was performed in 26 seconds using equal robot speeds and matching the RPM frequency.

D. X-ray validation

To validate the investigated behaviour in a clinical setting, the trajectory rolling was evaluated in the two phantoms previously mentioned in Section III-D.

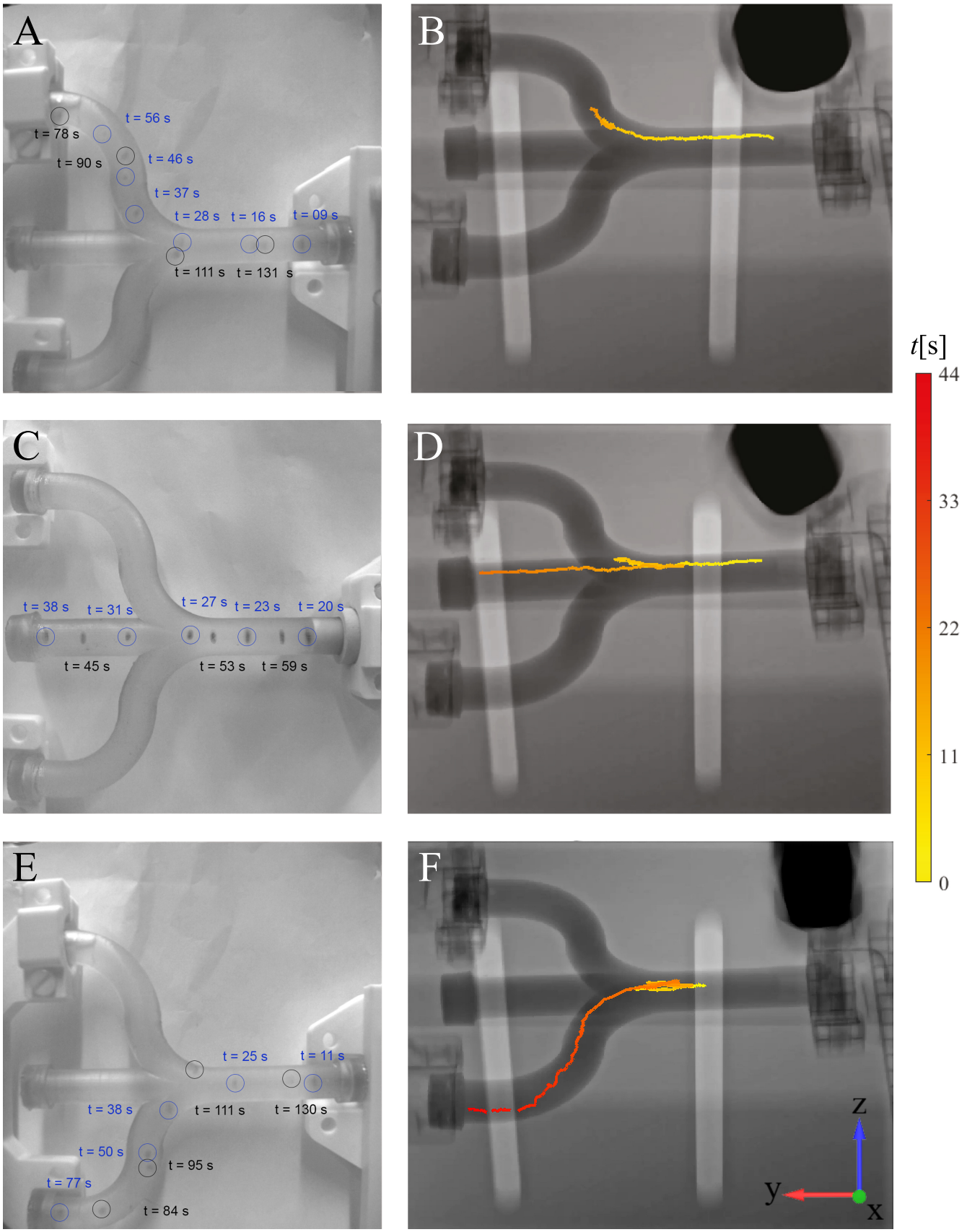

Fig. 7: Timestamped trials of trifurcation branches (left). Blue ellipses depict forward movement and black ellipses a backwards movement. X-ray validation of the tested branches is shown with a colorbar timescale (right).

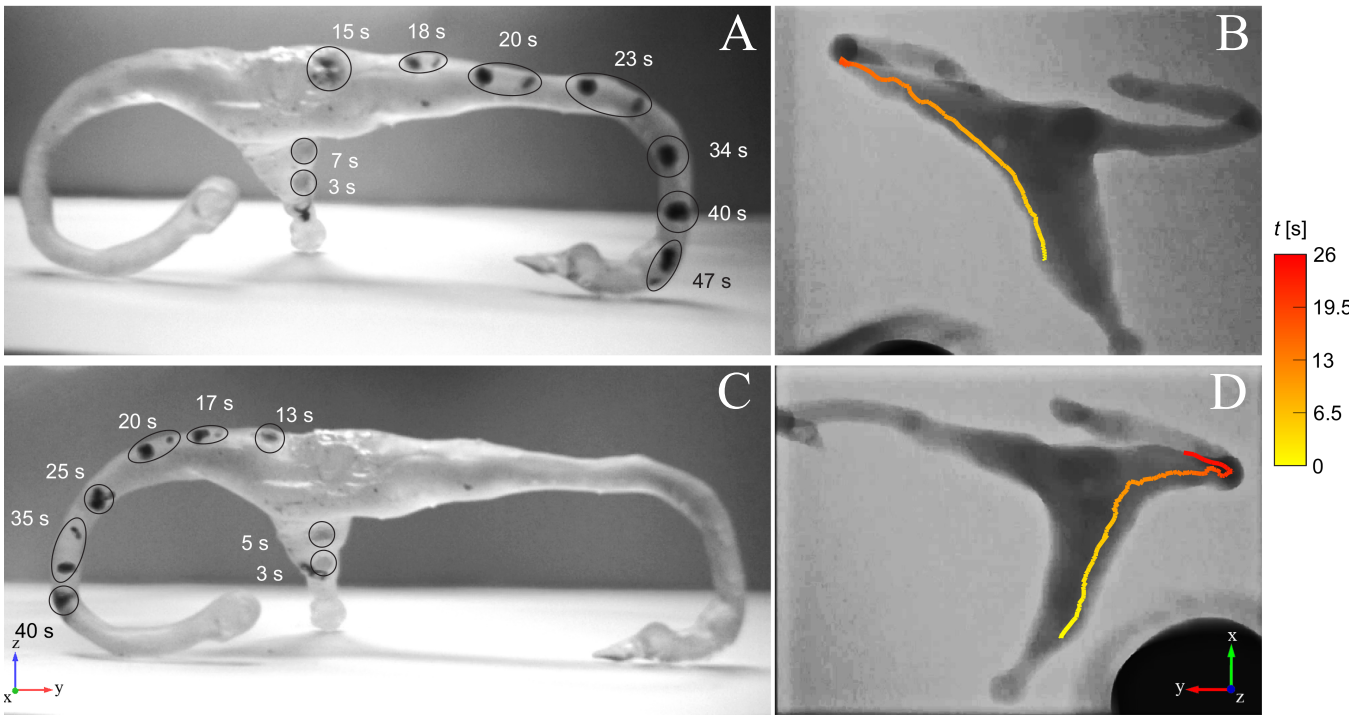

Fig. 8: Cluster trajectory over time captured by camera (left) and X-ray (right). The top figures show the trajectories in the right fallopian tube and the bottom figures the left fallopian tube. The ellipses display the positions in a certain timeframe of all parts associated with the main cluster when split. The color bar represents the time scale for the X-ray images in seconds.

For each branch of the trifurcation phantom, one trial was recorded as validation of the experiment mentioned in the previous section. The experiment was conducted using only the side-rolling method since ceiling rolling with cause the KUKA robot to collide with the Artis Pheno system (Figure 7).

The X-ray recorded video for the top branch was obstructed by the RPM, therefore not able to leave a trace in the figure. RPM intervention was sometimes necessary to control the position of the cluster with respect to the RPM, showing an oscillating behaviour in 7D and F.

During the experiment,5 successful trials were recorded and analysed for each fallopian tube of the reproductive tract. The rolling path and their trajectory planning are shown in Figure 8.

V. DISCUSSION

A. *IRONSperm clusters*

Due to the limited availability of clusters, only two clusters were used during the entirety of this research. It was assumed that negligible differences between the clusters would be of effect. However, the robustness and size affected the rolling behaviour substantially. This damages the repeatability of the experiments, thus questioning the relevance of the characterisation of the clusters. The performance of the clusters was relatively constant when adhering to the same cluster without transporting it to another vessel. Nonetheless, the clusters are susceptible to entangling with waste and particles present in the vials (see Figure 9), impeding the performance permanently. Because of this, the first cluster used for the inclined surface and actuation distance experiment (Section IV-A) was not viable for further use in other experiments and had to be exchanged for another cluster of the same nanoparticle concentration.

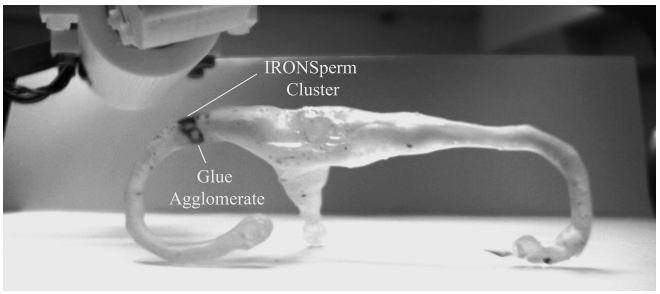

Fig. 9: Cluster entangles with glue debris

Noticeable differences in size and shape between the clusters resulted in different approaches to the trajectories and actuation distances applied. Interestingly, the second, larger, cluster responded better to the rotating magnetic field and was more resilient to discontinuities in the rolling surface. Furthermore, it was easier to localise using camera feedback. In turn, the first cluster was more robust, leaving little to no trail of separated clusters in the process. As mentioned in Section 1, smaller clusters affect the rolling behaviour of the main cluster when they remain in close proximity. Not only

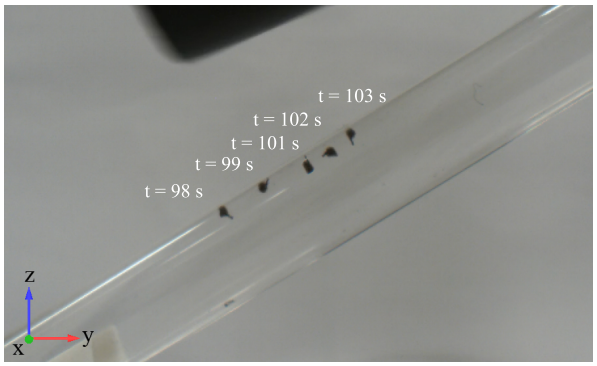

Fig. 10: The main cluster uses a smaller cluster as a 'setting pole' to propel itself forward, resulting in a quicker but more inconsistent motion. The cluster moves in an ascending motion under a 30-degree angle.

in terms of additional forces acting on the body, but also in terms of mechanical pushing and setting pole behaviour as seen in Figure 10. These factors influenced the results in this paper greatly. The results of these separate experiments should thus not be compared to each other, but conclusions should rather be interpreted from the individual experiments. This paper would therefore recommend focussing on the control of clusters rather than characterisation since there is no form of standardisation possible for the current clusters.

B. KUKA and RPM

This paper aimed to research the available methods for vertical locomotion of IRONSperm and compare them to select the most appropriate methods. The main reason for this was the limited joint space that the KUKA robot was able to reach. Braks proposed increasing magnet size and consequently the magnetisation of the cluster for a broader range of actuation distances [18]. This would allow for a more free orientation of the KUKA robot, resulting in easier and more effective trajectories for IRONSperm guidance. This research confirms the necessity of this proposal since the possible configurations of the KUKA robot were the largest limiting factor for more extensive research.

The KUKA robot differentiates between joint and linear speed. When applying equal speeds for both parameters, the cluster was not able to track accurately since the linear movements would occur much quicker than the joint movements. This required a sense of trial and error to find the most appropriate combination for ideal tracking. Perhaps this might be a focus of interest for future research since these parameters are important for accurate tracking of the cluster.

This paper mostly explored the behaviour of IRONSperm upon positively inclined surfaces and therefore requires more research to find the discrepancies between descending and ascending motions. The gravitational force acting on the cluster often caused the cluster to roll in front of the magnet, losing the magnetic coupling with the RPM. Since the trajectories were mostly automated, the system often experienced difficulty with regaining magnetic pulling force on the cluster. The direction of the RPM therefore had to be changed sometimes to maintain the position of the cluster within the minimum actuation distance necessary to pull the cluster towards the solid boundary. However, this will not be possible in clinical settings since real-time imaging of the cluster is not yet a reality. Further investigation should therefore focus on refining the existing trajectories in terms of speed and automation.

C. Experimental validity

The results of the experiment explained in Section IV-A are performed in Tracker [29]. This program requires a measurement step and a reference coordinate system. Uncertainties are possible within these arbitrary parameters. The method used was applied consistently so the results are valid when interpreted relatively, sharing interest with the scope of this research. For subsequent experiments in Sections IV-B and IV-D, a measurement scale was always implemented to nullify errors caused by this potential discrepancy.

Moreover, the previous section gave insight into the event where the pulling force could not compensate for the gravitational force acting on the cluster, causing it to fall. As a consequence, trials were not performed threefold for the 60- and 75-degree angles in the experiment performed in Section IV-A. This resulted in more biased means and standard deviations.

On another note, the results for the pitchfork trials mentioned in Section IV-C were conducted in two similar versions of the trifurcation phantom. The phantom used in the trials for side-rolling was an updated version of the other, removing constructions remains of the resin printing process. The phantom in the side-rolling trials was however found to contain glue, resulting in low-performing clusters. Therefore, the earlier version was used for the ceiling rolling trials.

The trajectory of the KUKA robotic arm proved to be much slower for side-rolling, especially when rotating the joint where the RPM was mounted. This resulted in far slower tracking for the cluster in the side-rolling trials, mainly in the areas where the cluster was required to turn. In Figure 6 it is noticeable that the parts where the cluster rolls in a linear path occur much quicker than when the cluster rotates around its axis. When accounting for this discrepancy, the conclusion remains the same but has a smaller, yet substantial margin between the two investigated methods.

Lastly, as mentioned in Section II-F, the cilia propel zygotes towards the uterus. This peristaltic motion moves against the desired direction of the IRONSperm clusters. This impedes the motion of IRONSperm in the fallopian tubes. Moreover, the cilia are intended to prevent and obstruction of aggregation of sperm cells. It is however unclear if the cilia manage to disrupt the forces explained in Section II-A. The viability of IRONSperm in the fallopian tubes thus remains a challenge and requires more robust clusters with stronger actuation to overcome the motion-impeding events mentioned above.

VI. CONCLUSIONS

This paper researched the available methods of vertical rolling for IRONSperm microrobot clusters in an attempt to select the most appropriate method in terms of robot manoeuvrability and rolling speed. Multiple experiments were used to investigate this research objective. The inclination angle of a rolling surface has a negligible effect on the rolling velocity. A slight regressing trend is noticed when increasing actuation distance under a sloped surface. Furthermore, side rolling and ceiling rolling acquire similar speeds under both horizontal and inclined situations. Ceiling rolling is found to be slightly quicker and is therefore recommended as the most appropriate method for situations where the clusters must roll on a positively angled inclination. This result was validated in a trifurcation phantom, showing much quicker locomotion for ceiling rolling. However, in terms of manoeuvrability in descending branches or horizontal branches, side rolling is found to be the most effective method of locomotion. These trajectories were also successfully validated in the trifurcation phantom. Through the combination of the described methods, IRONSperm clusters were able to successfully navigate through an anatomically realistic phantom of the reproductive tract. Open loop control can be realised in an enclosed lumen for IRONSperm clusters, paving a promising future for this innovation.

REFERENCES

[1] Matulonis, U., Sood, A., Fallowfield, L. et al. Ovarian cancer. Nat Rev Dis Primers 2, 16061 (2016). https://doi.org/10.1038/nrdp.2016.61

[2] F. Amant, P. Moerman, P. Neven, D. Timmerman, E. Van Limbergen and I. Vergote, "Endometrial cancer" in *The Lancet* vol. 366, no. 9484, pp. 491-505, DOI: 10.1016/s0140-6736(05)67063-8

[3] Reid, F., Bhatla, N., Oza, A., Blank, S., Cohen, R., Adams, T., Benites, A., Gardiner, D., Gregory, S., Suzuki, M., Jones, A., "The World Ovarian Cancer Coalition Every Woman Study: identifying challenges and opportunities to improve survival and quality of life" in *International Journal of Gynecological Cancer*, vol. 31, pp. 238 - 244, 2020 https://doi.org/10.1136/ijgc-2019-000983.

[4] Morice, P., Leary, A., Creutzberg, C., Abu-Rustum, N., Darai, E., "Endometrial cancer" in *The Lancet*, vol. 387, pp. 1094-1108, 2016, https://doi.org/10.1016/S0140-6736(15)00130-0.

[5] Jinhua Li, Lukas Dekanovsky, Bahareh Khezri, Bing Wu, Huaijuan Zhou, Zdenek Sofer, "Biohybrid Micro- and Nanorobots for Intelligent Drug Delivery" in *Cyborg Bionic Syst.*, 2022;2022:DOI:10.34133/2022/9824057

[6] S. Nocentini, C. Parmeggiani, D. Martella, D. S. Wiersma, "Optically Driven Soft Micro Robotics" in *Advanced Optical Materials*, vol. 6, 2018, https://doi.org/10.1002/adom.201800207

[7] N. Pellicciotta, O. S. Bagal, V. C. Sosa, G. Frangipane, G. Vizsnyiczai, R. D. Leonardo, "Light Controlled Biohybrid Microbots" in . *Adv. Funct. Mater.*, 2023, vol. 33, https://doi.org/10.1002/adfm.202214801

[8] L. Sun, Y. Yu, Z. Chen, F. Bian, F. Ye, L. Sun, et al. "Biohybrid robotics with living cell actuation" in *Chem. Soc. Rev.* Vol. 49, No. 12, pp. 4043-4069, 2020

[9] F. Iberite, L. Vannozzi and L. Ricotti, "Biohybrid Microrobots" in *Springer International Publishing* 2022, DOI 10.1007/978-3-030-80197-7-13

[10] Yunus Alapan, Oncay Yasa, Berk Yigit, I. Ceren Yasa, Pelin Erkoc, Metin Sitti "Microrobotics and Microorganisms: Biohybrid Autonomous Cellular Robots" in *Annual Review of Control, Robotics, and Autonomous Systems*, vol 2, No. 1, pp. 205-230, 2019

[11] Zhu, S., et al. "Biohybrid magnetic microrobots: An intriguing and promising platform in biomedicine." in *Acta Biomaterialia*, vol. 169, pp. 88-106, October 2023

[12] Yang, L. and L. Zhang, "Motion Control in Magnetic Microrobotics: From Individual and Multiple Robots to Swarms." in *Annual Review of Control, Robotics, and Autonomous Systems*, vol. 4, no. 1, pp. 509-534, 2021

[13] L.-J. W. Ligtenberg, I. A. A. Ekkelkamp, F. Halfwerk, C. Goulas, J. Arens, M. Warle, and I. S. M. Khalil, "Helical Propulsion in Low-Re Numbers with Near-Zero Angle of Attack", in *Proceedings of the IEEE International Conference on Intelligent Robots and Systems (IROS)*, Detroit, Michigan, USA, October 2023.

[14] Yousefi, M., Nejat Pishkenari, H., "Independent position control of two identical magnetic microrobots in a plane using rotating permanent magnets" in *J Micro-Bio Robot* vol.17, 59–67, 2021, https://doi.org/10.1007/s12213-021-00143-w

[15] T. W. R. Fountain, P. V. Kailat and J. J. Abbott, "Wireless control of magnetic helical microrobots using a rotating-permanent-magnet manipulator," in *2010 IEEE International Conference on Robotics and Automation, Anchorage, AK, USA*, pp. 576-581, 2010, doi: 10.1109/ROBOT.2010.5509245.

[16] P. Ryan and E. Diller, "Magnetic Actuation for Full Dexterity Microrobotic Control Using Rotating Permanent Magnets" in *IEEE Transactions on Robotics*, vol. 33, no. 6, pp. 1398-1409, Dec. 2017, doi: 10.1109/TRO.2017.2719687.

[17] Middelhoek, K. I. N. A., et al., "Drug-Loaded IRONSperm clusters: Modeling, wireless actuation, and ultrasound imaging." in *Biomedical Materials*, vol 17, no.6, 2022

[18] Braks, R.J.M., "Motion control of IRONSperm clusters in a vascular model", 2023

[19] V. Magdanz, I. S. M. Khalil, J. Simmchen, G. P. Furtado, S. Mohanty, J. Gebauer, H. Xu,A. Klingner, A. Aziz, M. Medina-Sánchez, O. G. Schmidt, S. Misra, "IRONSperm: Sperm-templatedsoft magnetic microrobots" *.Sci. Adv.*, vol. 6, 2020

[20] Magdanz, Veronika Cumming, Jack Salamzadeh, Sadaf Tesselaar, Sven Alic, Lejla Abelmann, Leon Khalil, Islam, "Influence of Nanoparticle Coating on the Differential Magnetometry and Wireless Actuation of Biohybrid Microrobots.", 2023, 10.1109/IROS55552.2023.10341258.

[21] M. M. Micheal, A. Adel, C. -S. Kim, J. -O. Park, S. Misra and I. S. M. Khalil, "2D Magnetic Actuation and Localization of a Surface Milli-Roller in Low Reynolds Numbers," in *IEEE Robotics and Automation Letters*, vol. 7, no. 2, pp. 3874-3881, April 2022, doi: 10.1109/LRA.2022.3148787

[22] Weber, L., "Frequency actuation influence on velocity of different concentrations IRONSperm in *in vitro* situation", 2023

[23] Bloxs, M., "A TRADE STUDY OF BIOHYBRID MICROROBOTS: COMPARING ACTUATION AND LOCALIZATION OF IRONSPERM", 2023

[24] Wu, L.C., Zhang, Y., Steinberg, G., Qu, H., Huang, S., Cheng, M., Bliss, T., Du, F., Rao, J., Song, G., Pisani, L., Doyle, T., Conolly, S., Krishnan, K., Grant, G., Wintermark, M., "A Review of Magnetic Particle Imaging and Perspectives on Neuroimaging" in *American Journal of Neuroradiology*, vol. 40, 206–212, 2019, https://doi.org/10.3174/ajnr.a5896

[25] Veronika Magdanz, Yusra Pervez, Mathilda LaBrash-White, Leendert-Jan W. Ligtenberg, Mohan Bloxs, Sadaf Mohsenkani, Maud Gorbet, Negin Bouzari, Hamed Shahsavan, Lianne Weber, H. Remco Liefers, Michiel Warle and Islam S. M. Khalil, "Sperm Cell Empowerment: X-Ray-Guided Magnetic Fields for Enhanced Actuation and Localization of Cytocompatible Biohybrid Microrobots", 2024

[26] Ko E, Song YJ, Choe K, Park Y, Yang S, Lim CH., "The Effects of Intravenous Fluid Viscosity on the Accuracy of Intravenous Infusion Flow Regulators" in *J Korean Med Sci*, vol. 37, no. 9, 2022 Mar 7. doi: 10.3346/jkms.2022.37.e71. PMID: 35257526; PMCID: PMC8901879.

[27] Ding, D., Shi, W. Shi, Y., "Numerical simulation of embryo transfer: how the viscosity of transferred medium affects the transport of embryos" in *Theor Biol Med Model*, vol. 15, no. 20, 2018, https://doi.org/10.1186/s12976-018-0092-y

[28] H. Ashraf, A.M. Siddiqui, M.A. Rana, "Fallopian tube analysis of the peristaltic-ciliary flow of third grade fluid in a finite narrow tube" in *Chinese Journal of Physics*, vol. 56, no. 2, 2018, pp 605-621, https://doi.org/10.1016/j.cjph.2018.02.001.

[29] Brown et al. (2023) Tracker version: 6.1.5. Available: https://physlets.org/tracker/

[30] The MathWorks, Inc. (2022). MATLAB version: 9.13.0 (R2022b). Accessed: January 01, 2023. Available: https://www.mathworks.com.

APPENDIX

A. Rolling Behaviour

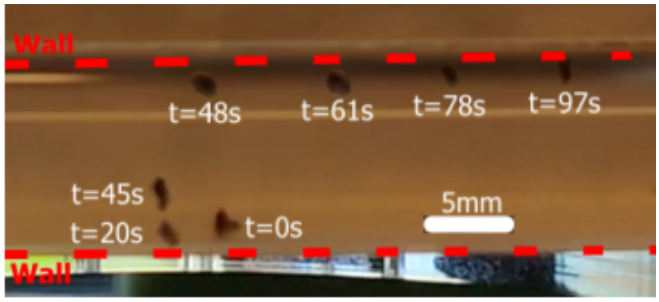

Fig. 11: Cluster with inadequate pulling force rolls on the bottom floor (left) and ascends when pulling force is applied, realising contact with the ceiling (right). [18]

B. KUKA paths

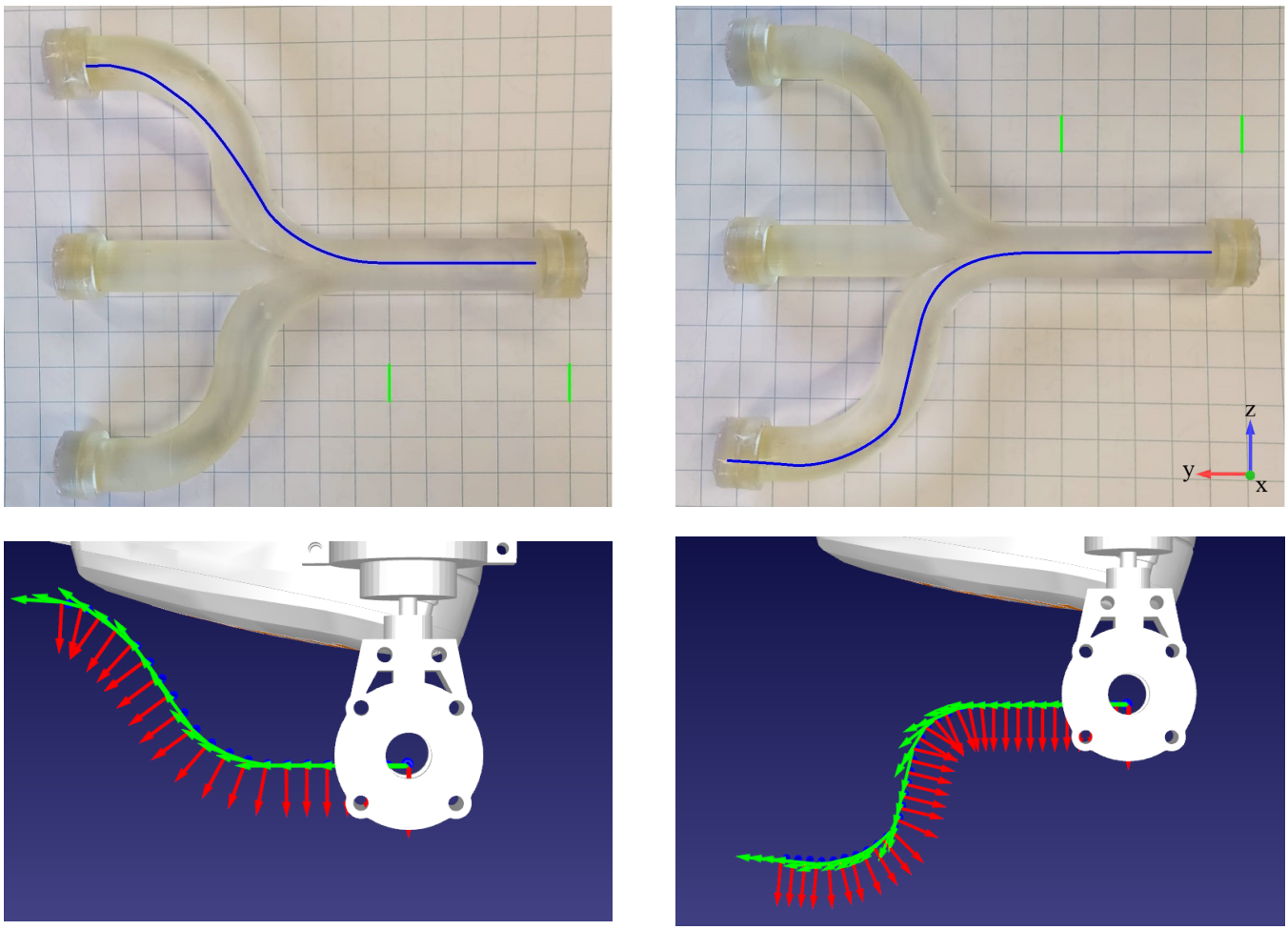

Fig. 12: The top images represent the templates used for trajectory planning in RoboDK. Python was used to convert the template to a trajectory. The green bars acted as a measure of 5 cm to scale the trajecotry in RoboDK. The bottom images display the resulting RPM paths in RoboDK used for the trials in Figure 7.

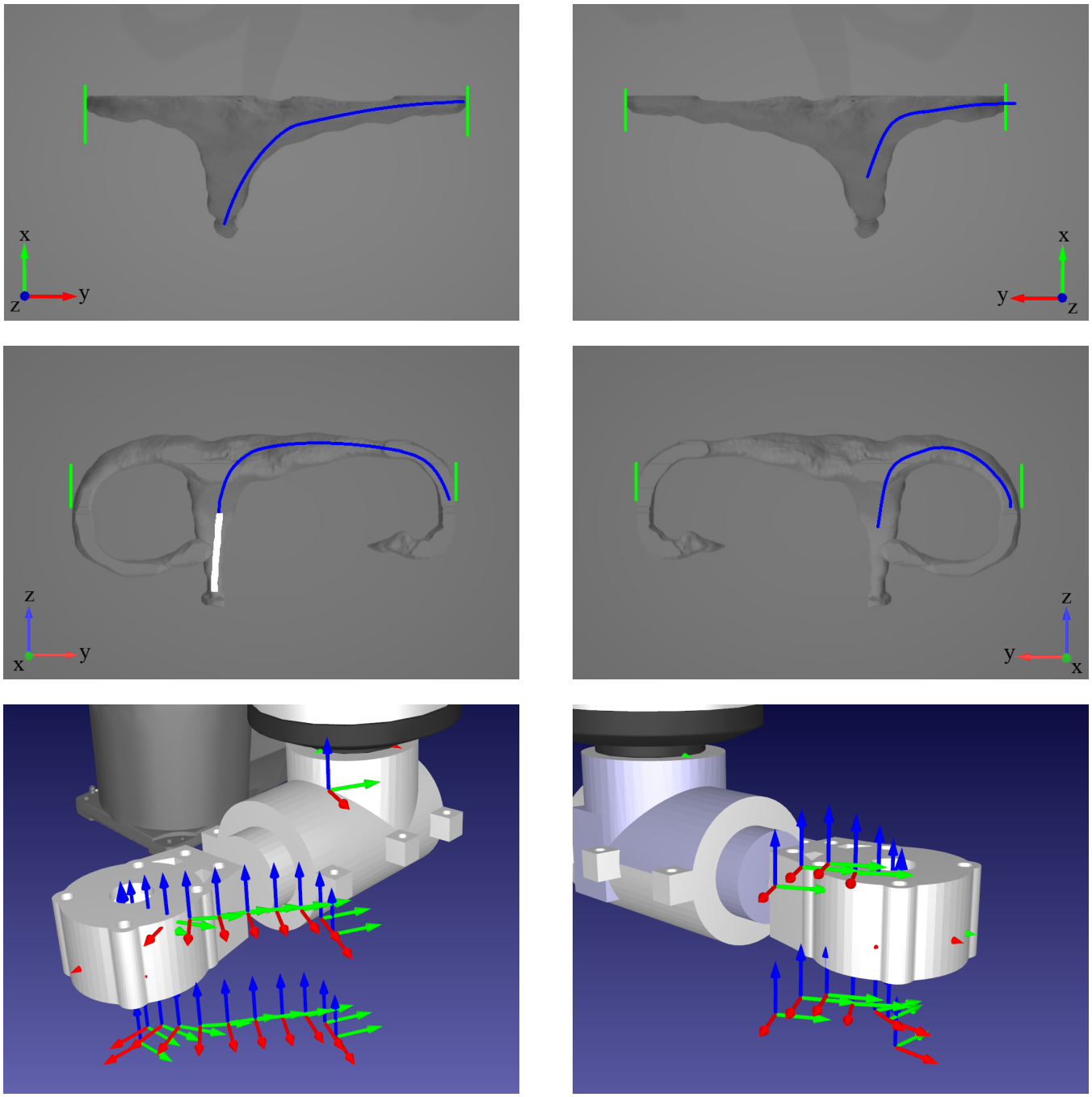

Fig. 13: The left images represent the templates and resulting KUKA path for the right branch of the reproductive tract. The right images for the left branch. Templates were made for two views, top view (top images) and front view (middle images). The trajectory was constructed using a 3D version of the one used in Figure12

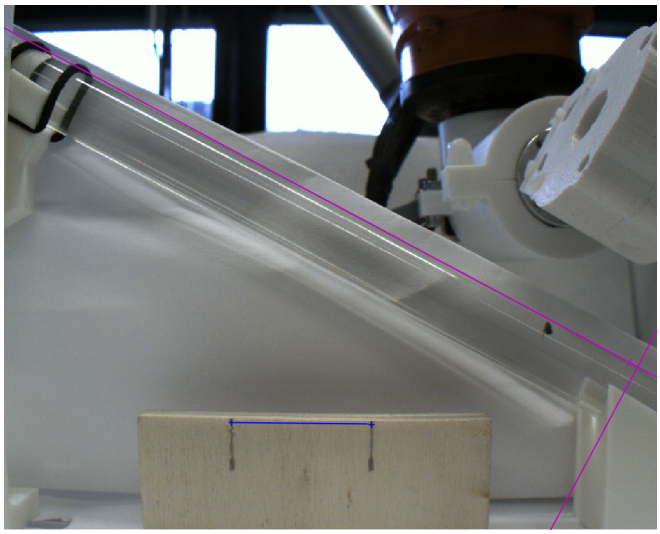

Fig. 14: The pink axes represent the arbitrary coordinate system. The x-axis was chosen to align with the 1D tube. For pitchfork experiments, the coordinate system was placed in the top left corner. The blue line indicated a measurement stick for the derivation of position to scale.

C. Tracker and Matlab analysis

The results retrieved from the experiments in Sections IV-AIV-BIV-C and IV-D were performed using a combination of Tracker and Matlab. The videos were first auto tracked in Tracker using a pixel template as a cluster and searching for this pixel template in all frames (see Figure 14). This resulted in the x and y positions of the cluster over time. This raw data was later processed in Matlab for further analysis. When speed was computed, areas in the data where the speed adopted a linear trend were used. The speed over this interval was calculated for each trial and the mean and standard deviation were calculated.

For the colorbar tracing figures the same method was applied for tracking. The x and y positions were overlayed with the first frame of the video. A colorbar was added to visualise time in the figure.